Battery internal resistance estimation using a battery balancing system based on switched capacitors

Cristina Gonzalez Moral[††], Diego Fernández Laborda[†], Lidia Sánchez Alonso[†], Juan Manuel Guerrero[†], Daniel Fernandez[†], Carlos Rivas[††] and David Díaz Reigosa[†]

† University of Oviedo. Dept. of Elect. Computer & System Engineering, Gijón, 33204, Spain

† † Electrotécnica Industrial y Naval, S.L. (ELINSA), 15008, A Coruña, Spain

cgonzalez@elinsa.org, dflaborda@uniovi.es, uo250173@uniovi.es, guerrero@uniovi.es, fernandezalodaniel@uniovi.es, crivas@elinsa.org, diazdavid@uniovi.es

***Abstract*— Battery Management Systems (BMS) are key components in battery storage systems in order to guarantee their safe operation and improve their performance, reliability and efficiency. BMS monitor critical parameters in the battery as State Of Charge (SOC), State Of Health (SOH) or temperature. Direct measure of SOC or SOH is not possible, while temperature, on the other hand, can be measure with different types of sensors. These sensors, although cost-effective, raise concerns regarding cabling, signal conditioning and acquisition systems, increasing cost, complexity and decreasing reliability. The internal resistor of the battery has already been successfully used to estimate these parameters. BMS can also include the function of balancing (equalizing) cells of a battery pack. Among all available equalizing systems, those based on switched capacitors are interesting due to their simplicity and easy scalability. This paper proposes an internal resistance (IR) estimation method for $LiFePO_4$ batteries using signals naturally produced by a Switched-Capacitor Equalizer (SCE). The IR will be used to estimate the battery temperature. It will be shown that the method can operate online and without interfering with the regular operation of the SCE.[1]**

Keywords*— *LFP/$LiFePO_4$ batteries, switched-capacitor equalizer, internal resistance estimation, temperature estimation.

I. Introduction

The use of battery-based Energy Storage Systems (ESS) has highly increased in the last decades [1]. They can be found in a broad range of applications, such as electric vehicles (EV) [2], smart grids [3], aerospace applications [4] and all kinds of small appliances applications as mobile devices [5].

There is a wide variety of rechargeable batteries (secondary batteries) technologies that could be used for ESS, as nickel-cadmium (NiCd), Pb-acid or lithium-ion (Li-ion). Among these, Li-ion Batteries (LIBs) are one of the most appealing batteries for high capacity ESS due to their high energy density, good temperature operation range, low self-discharge, high efficiency and high cell voltage compared with NiCd or Pb-acid [5], [6].

Since the cell voltage and/or current in any of these cases is low compared with typical industrial requirements, battery packs are built stacking cells in series and/or parallel configurations [2], [6]. Manufacturing tolerances, temperature differences, cell distribution inside the pack (which affects the battery temperature), among other reasons, result in voltage imbalances among cells during normal pack operation. These imbalances accelerate the aging of cells and result in an increase of the internal battery resistance and a decrease of its capacity. Mismatches in voltage among cells also increase the internal battery temperature, decreasing therefore operation safety [7], [8]. Thermal behavior is also heavily affected by how the battery is employed in terms of current demand and sudden load changes [9]. Active materials in the LIBs can be potentially damaged in the case of overvoltage or undervoltage [10], [11]. For all these reasons, BMS are needed to increase the overall safety of the system: monitor critical parameters as temperature, SOC or SOH [3]-[13], control operational conditions and cell balancing, extend the life of the battery and ensure a safe range of operation for all the cells forming the pack [6], [12].

One of the main features of BMSs is the equalizing of cells, which allows to maximize the energy extracted from the battery pack without compromising safety [11]. Among proposed equalizers in the literature, the SCEs [11], [14]-[18] are one of the most appealing techniques to equalize single cells due to its low cost and simplicity. They can be used to balance all kinds of battery chemistries, as Pb-acid or nickel-based [14] or LIBs [11], [17], [18]. Unlike other equalizers, SCEs can work effectively both during battery charging or discharging [7]. SCEs equalize cells in terms of voltage, which means that there will be energy transfer between the cells while there is voltage difference among them.

Another important feature of a BMS is battery temperature knowledge. Batteries' temperature can be directly measured using temperature sensors [19]. These sensors, although cheap, raise concerns regarding cabling, signal conditioning and acquisition systems, increasing cost, system complexity and the number of elements susceptible to failure [20], [21]. As an alternative, the batteries' temperature can be estimated. Temperature estimation methods based on the dependency of a battery parameter with its temperature are the most popular [19]-[23]. On the other hand, since SOC and SOH cannot be directly measured, estimation methods must be implemented [12].

Several methods to estimate battery parameters can be found in the literature: the real part [19], [21], the imaginary part [20], the magnitude [21] and the phase shift [23] of the battery impedance being the most relevant. This kind of methods estimate the battery impedance from the battery terminal voltages and currents when the battery is being

[1] This work was supported in part by the Research, Technological Development and Innovation Programs of the Spanish Ministry Economy and Competitiveness, under grant MINECO-17-ENE2016-80047-R, by the "Oviedo Siembra Talento" program of the Oviedo City Council and by the Government of Asturias under project IDI/2018/000188 and FEDER funds.

connected to a power converter which has the capability of injecting some high-frequency signal superimposed on top of the fundamental DC current component; i.e. these methods work in an analogous way to the Electrochemical Impedance Spectroscopy (EIS) analysis [20] but only for a single frequency.

This paper, which is the extended version of the conference paper [1], proposes an on-line battery IR [24] estimation method, i.e. during cell balancing, for SCEs. The IR of the battery is estimated using signals produced by the SCE regular operation; the IR will be used for cell temperature estimation, therefore this method cannot be directly compared to [19]-[23]. Nevertheless, and since battery packs can be connected to the rest of the system using a power converter, both estimation methods could be employed simultaneously, thus increasing the reliability of the temperature estimation. Besides, and as it will further explained in section IV, once the cells are equalized, there is no voltage difference among them, nor equalization current, meaning that the IR cannot longer be estimated with the proposed method. Due to this, combining the proposed method in this paper with the ones proposed in [19]-[23], in those cases where a power converter is employed to connect the battery pack to the rest of the system, could be a way of expanding the cell temperature estimation. The current level and SOC could also affect the proposed method, this will be analyzed in section IV.

The article is organized as follows: the basis of SCEs are presented in section II; electrical modeling of batteries are discussed in section III; the proposed method for battery IR estimation is presented in section IV; simulations and experimental results are shown in sections V and VI respectively; conclusions are finally presented in section VII.

II. Switched-Capacitor Equalizer

This section presents a brief review of different equalizing methodologies, focusing on SCEs. Battery/cell equalizers extract energy from the most charged cell of a battery pack and either dissipate or transfer it to a less-charged cell. The first method is known as passive balancing and the second as active balancing. Passive balancing is relatively inexpensive and easy to implement, although dissipating excessive energy makes it inefficient. Due to this, recent research efforts are focused on active balancing methods. Methods for active balancing can be classified according to different criteria, as the connections between the cells (cell-to-cell, pack-to-cell, cell-to-pack…) or according to the circuit topology (shunting, shuttling or energy conversion methods) [7], [12]. Shunting methods transfer the energy from one cell to another without any external energy storage device, unlike shuttling methods that use external energy storage devices, e.g. capacitors, inductors or other batteries. The so-called energy conversion methods [7] use isolated converters for equalizing the cells. This solution is the most expensive among them and often used to balance packs of cells, while the other two are more suitable to equalize single cells.

Among shuttling active balancing methods, one of the most appealing methods to equalize single cells is the switched capacitor equalizer [14], due to its low cost and simplicity. This cell-to-cell equalizer balances the voltage of N cells with N-1 capacitors and 2N switches, see Fig. 1a. The switches continuously work during regular operation of the battery with a fixed duty cycle of 50% but the corresponding dead time to avoid shortcircuit, alternating ON/OFF states between switches "a" and "b". This results in a very easy system that can work without any control strategy: there will be energy transfer between the cells if there is a voltage difference among them. This can be seen in Fig. 1b, where *Ts* is the switching period and *dt* the dead time. This way, each capacitor is connected half of the switching period in parallel with one cell and the second half with an adjacent cell, transferring energy from the one with the highest voltage to the one with the lowest voltage. This is schematically shown in Fig. 1c assuming VB1 > VB2 > VB3. In the state 1 (in red), B1 charges C_{12} and B2 charges C_{23}, i.e. they are connected in parallel, and in state 2 (blue), C_{12} discharges over B2 and C_{23} discharges over B3.

The main advantages of this equalizer are that it does not require control, it is fully scalable, cost-effective and easy to implement. In addition, and unlike other methods, it can work effectively both in charge and discharge [7]. As a drawback, cells only transfer energy effectively to their adjacent ones, so the energy might need to flow through a large number of cells, which increases the losses and the equalization time [11]. Another drawback is that the equalization speed depends on the voltage difference, so the process becomes slower as the voltage difference decreases. Note that this equalizer may induce losses if the switching is maintained once the cells are voltage balanced. To avoid this, a voltage threshold to start and stop the equalization may be selected. Since SCEs can be used with different types of battery chemistry [14], the selection of this threshold will depend both on the application and the cells that are being balanced. For example, when equalizing lead-acid cells the threshold can be higher than when equalizing $LiFePO_4$, since the latter has a much flatter SOC-OCV curve [12]. This threshold will also be related to the resolution of the acquisition system, as will be explained in section VI. It can be concluded that it is not straightforward to give a threshold figure valid for any battery chemistry/application.

A prototype for an SCE to balance four cells is shown in Fig. 1d. This prototype will be used for the experimental verification of the proposed battery IR estimation method.

The SCE from Fig. 1a can have large equalization time, especially if the capacity of the cells is high or they are extremely unbalanced. However, it is expected that this time is reduced if the SCE is permanently connected, since it will not allow large unbalances among cells. To reduce this time, different SCE topologies have been proposed. These equalizers improve the equalization time at the price of increasing the number of components used or the loss of modularity. These alternative SCE topologies are briefly analyzed in the following paragraphs [11], [14]-[18].

A. Switched-Capacitor Equalizer Topologies

-Basic switched-capacitor equalizer [14]**:** Fig. 1. Explained earlier in this section.

-Double-tiered switched-capacitor equalizer [11], [15], [16]:Fig. 2. An extra capacitor bridges the capacitors in the first row, so batteries have two paths to exchange charge, reducing the equalization time. As a drawback, there is a need for adding an extra capacitor to the system, which must withstand the combined voltage of all the capacitors, compromising the scalability of the topology.

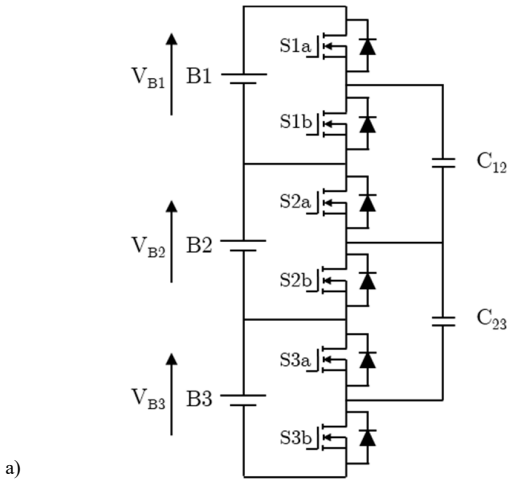

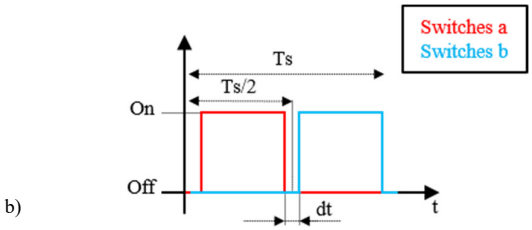

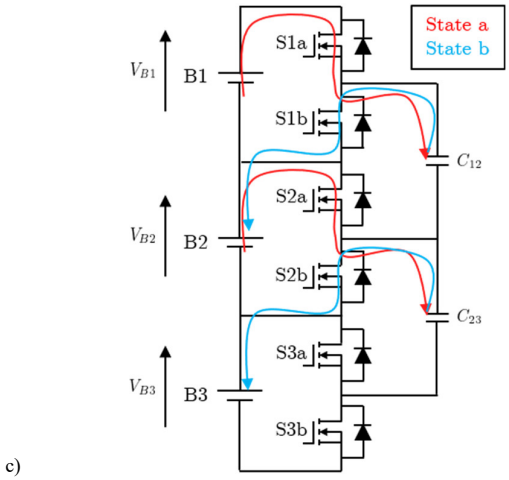

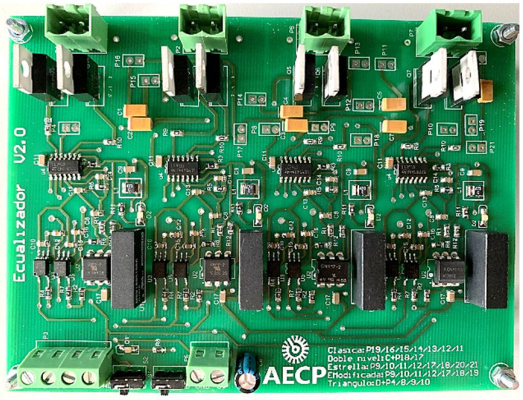

Fig. 1.- Switched capacitor equalizer with 3 cells, a) schematic with 3 cells, b) switching function, c) paths for the energy at both switching states, d) prototype for balancing up to 4 cells.

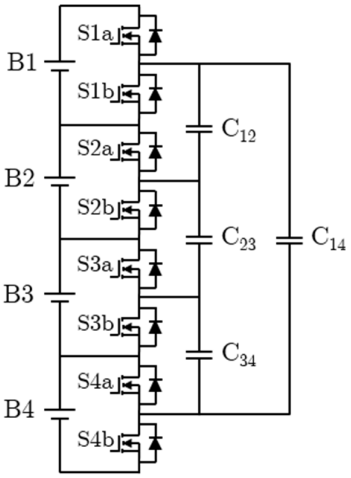

Fig. 2.- Double-tiered switched-capacitor equalizer.

-Chain structure using additional switches or capacitors [11]: Fig. 3. Requires four additional switches compared to the double-tiered SCE, top and bottom cells become therefore adjacent, forcing them to exchange energy between them and their adjacent cells only, and not with all the cells in the pack as in the previous case. The scalability of this topology is compromised as in the previous case since the voltage that the new switches must withstand is the same as the whole battery pack.

-Star-structured switched-capacitor equalizer [15]: Fig. 4 left. It requires one additional capacitor respect to the classic proposal and connects the capacitors in a star-structure that allows the interconnection of all the cells at the same time, which decreases the equalization time (making it independent of the initial imbalance status of the string) and efficiency. As a drawback, the scalability is again compromised because the voltage that each capacitor must withstand is different. A variation of this equalizer with one less capacitor can be seen in Fig. 4 right, [15] and [17].

-Delta structured switched-capacitor equalizer [18]: Fig. 5. This equalizer adds capacitors in such a way that there is always one capacitor connecting any two cells, allowing the interconnection of all the cells at the same time. As the double-tiered SCE, it maintains the number of switches but

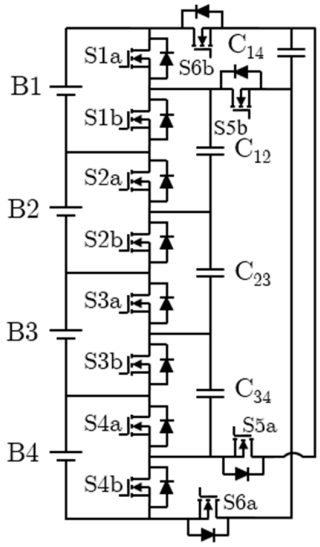

Fig. 3.- Chain structure using additional switches or capacitors.

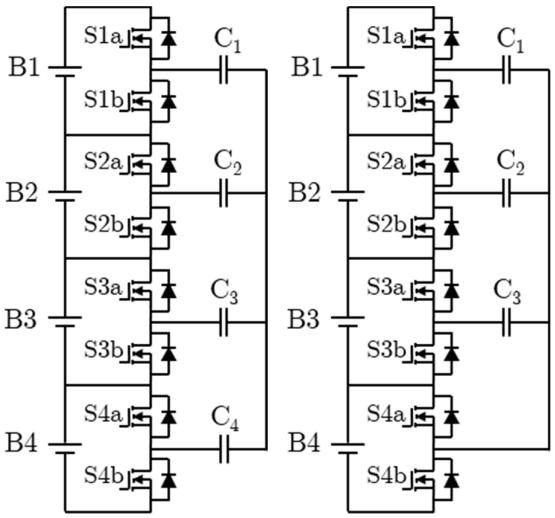

Fig. 4.- Star-structured switched-capacitor equalizer (left) and Star-structured switched-capacitor equalizer with one less capacitor (right).

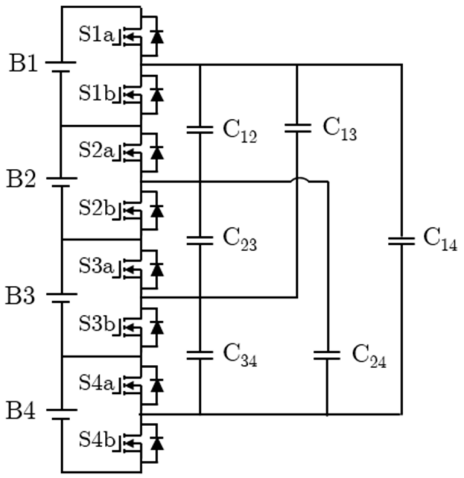

Fig. 5.- Delta-structured switched-capacitor equalizer.

increases the number of capacitors (in a higher number) while reducing the equalization time. The voltage that each capacitor must hold is different and dependent on the cells they are bridging.

A summary of the SCEs presented in this section is given in Table I, which shows a comparison among SCEs based on the number of switches and capacitors depending on the number of series-connected cells (N), if the equalization time varies with a change in the position of the cells and if the capacitors can be all equal or not depending on the voltage that they should withstand.

The previous discussion considered only balancing systems based on switched capacitors. They all have in common the same working principle, being cost-effective solutions easy to implement thanks to the absence of control. The main difference among them is the number of components and their connection, which changes the equalization time. There are more complex systems based in the same principle that combine inductors and capacitors to improve the performance in terms of speed and losses, such as achieving zero-current switching [25]. However, the increased difficulty in the design and number of components make them impractical for low-cost applications.

TABLE I. COMPARATIVE OF DIFFERENT SWITCHED-CAPACITOR METHODS

	Switches	Capacitors	Variable equalization time	Equal capacitors
SCE classic [14]	2N	$(N-1)$	YES	YES
Double-tiered [11][15][16]	2N	$(N-1)+1$	YES	NO
Chain structure [11]	2N+4	$(N-1)+1$	YES	YES
Star-structure [15][17]	2N	N or $(N-1)$	NO	NO
Delta-structure [18]	2N	$\sum_{i=1}^{i=N-1}(N-i)$	NO	NO

III. ELECTRICAL EQUIVALENT BATTERY MODEL

There are several ways of modeling the battery behavior: electrochemically (complex and difficult to obtain), mathematically (abstract and application-focused) and electrically (electrical equivalent models based on a combination of electrical passive elements). The latter are the most appealing due to their intuitiveness and computational burden [9], [26]. Among electrical models, the Randles [20], [26]-[28], see Fig. 6, and the Thèvenin [9], [26], [29], [30], see Fig. 7, models, are the most commonly used.

The Randles model (Fig. 6a) is obtained from the EIS, a standard methodology for battery characterization. It consists of applying AC voltage to the battery and measure the resulting current to estimate the impedance at different frequencies (Fig. 6b) [27], [28]. Each range of frequencies is dominated by different phenomena in the battery (diffusion effect, solid-electrolyte interface (SEI) resistance, metal collectors, etc.) [20].

In Fig. 6a, Z_w represents the Warburg impedance, which accounts for the diffusion phenomena (low frequencies). The RC circuit corresponds to the electrolyte and SEI resistance on the anode. Finally, R_i is the IR, point in Fig. 6b when the battery impedance changes from capacitive to inductive [20], [27]. Fig. 6b shows the EIS analysis (Nyquist plot) of the $LiFePO_4$ cell used in this paper; the x-axis represents the resistance and the y-axis the reactance (sign reversed), while each point in the graph corresponds to a different frequency.

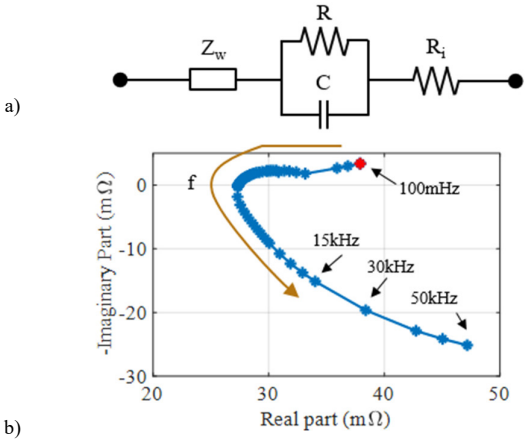

Fig. 6.- Randles equivalent model derived from the Electrochemical Impedance Spectroscopy (EIS) analysis, a) Circuit, b) Nyquist plot.

The frequency increases following the arrow direction where the red point indicates the smallest analyzed frequency.

On the other hand, Thèvenin model, see Fig. 7a, can be obtained from the battery response to a current step; parameter identification is obtained from the voltage transient response, see Fig. 7b [29]. In Fig. 7b, R_i is the cell IR, accounting for the resistance of the contacts, terminals, collectors, electrodes, and electrolyte, while R_D and C_D model the dynamic response, resulting from the effect of diffusion and charge transportation. Finally, C_{SOC} models the battery capacity, C_{SOC} voltage representing the battery Open Circuit Voltage (OCV) [26], [30].

The transfer function of this model is shown in (1). The first term on the right-hand side of (1) corresponds to the IR, Ri, and is obtained from the initial response to the current step, see Fig. 7b. The second term on the right-hand side of (1) is the dynamic RC circuit, a first-order system corresponding to the exponential part of the voltage variation, see Fig. 7b. The last term on the right-hand side of (1) is C_{SOC}, a pole at the origin, which accounts for the continuously increasing slope in the voltage in Fig. 7b due to a constant current.

$$G(s)=\frac{V_{bat}(s)}{I_{bat}(s)}=R_i+\frac{R_D}{1+R_D C_D s}+\frac{1}{s}C_{SOC} \qquad (1)$$

Among these models, the Thèvenin one is the most appropriate for battery parameter identification using an SC equalizer, since the process for extracting the parameters involved in (1) (i.e. step response) are similar to the steps produced in the battery as a result of the SC switching.

IV. Battery Parameter Identification Based on SC Equalizers

This section presents the proposed method for battery IR estimation using signals produced by the SCE operation. A simplified scheme of an SCE is presented in Fig. 8a, where the battery and SCE parameters are shown in Table II. The circuit is connected at the instant t_i, and the waveforms resulting from this connection are shown in Fig. 8b, which resemble SCE waveforms. Note that applying an impulse in the voltage is analogous to applying an impulse in the current from the point of view of battery parameter estimation [29].

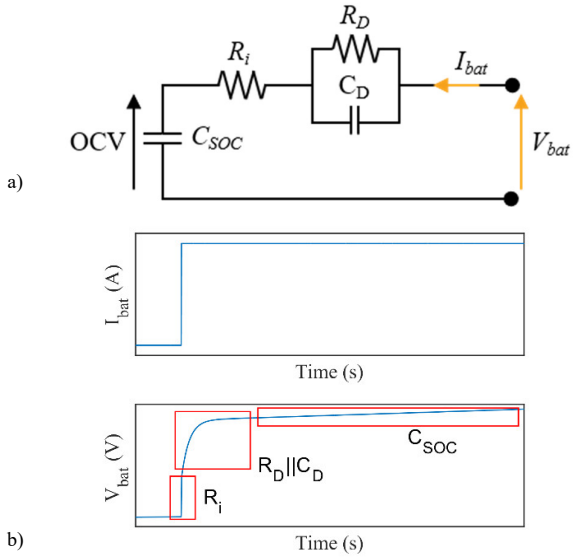

Fig. 7.- a) Thèvenin equivalent model of a battery, and b) response of a battery to a current step.

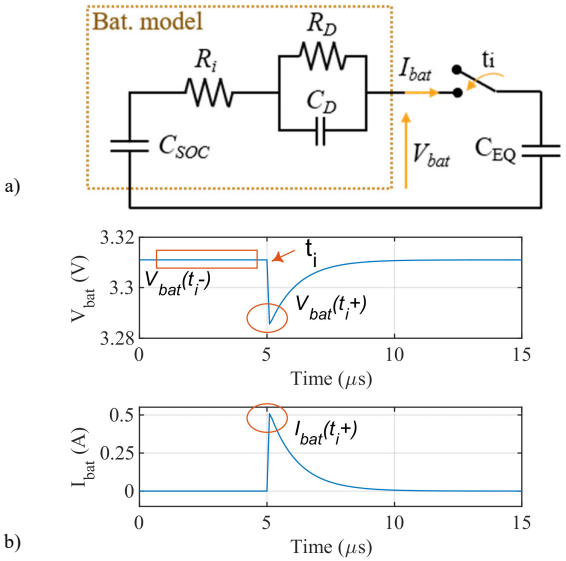

Fig. 8.- a) Simplification of the SCE, modeling the battery as a first-order Thèvenin model, and b) resulting voltage and current waveforms.

Before the switch connection, there is no current circulation, so the voltage measured (V_{bat} in Fig. 8a) is the OCV (the voltage in the capacitor C_{SOC}). After the switch connection, there is a current flowing from/to the battery and consequently a voltage drop in the battery IR, R_i, exists. Therefore, R_i can be obtained from (2). $V_{bat}(t_i+)$ and $I_{bat}(t_i+)$ are the voltage and current right after the connection instant (t_i), see Fig. 8b, while $V_{bat}(t_i-)$ is the OCV (see Fig. 8b).

$$R_i=\frac{\left|V_{bat}(t_i-)-V_{bat}(t_i+)\right|}{\left|I_{bat}(t_i+)\right|} \qquad (2)$$

When using this SCE, two different currents may be superimposed, the current through the series-connected cells due to the charge/discharge of the battery, and the transient current due to the switching of the SCE. The first current, which will be DC, can be controlled provided that the battery is connected to a power converter. The second current cannot be controlled since it depends on the voltage difference between the cells been equalized. As seen in [21], the current level may affect slightly the IR estimation. This effect can be compensated using an analogous procedure as shown in [21], using a look-up table to decouple the current level effect on the estimation.

The IR measured in batteries can change depending on the frequency of the signal used for measurement. The IR measured using the proposed procedure is a high-frequency resistance since the transient response of the battery is used for the estimation. At high frequencies, the IR is dominated by the leads and metal collectors of the battery [30]. Due to this, SOC is not expected to affect the estimation, since it does not affect the high-frequency impedance on LIBs [21], [23].

TABLE II. Battery Model Parameters

Parameter	Value	Parameter	Value
R_i	50 mΩ	C_{SOC}	19 kF
R_D	6.7 mΩ	C_{EQ}	22 µF
C_D	48F		

SCEs can effectively work both during the charge and discharge of the cell [7]. In case the battery is being charged or discharged, the method is similarly applied with the exception of the current in Fig. 8b will include this charging/discharging current. In this case, a more general equation, (3) should be used. $I_{bat}(t_i)$ is the current before the commutation, in this case, the current been charging/discharging the battery. The absolute value allows, as in (2), the equation to be used for both charging and discharging. The results remain unchanged.

$$R_i = \frac{|V_{bat}(t_i-) - V_{bat}(t_i+)|}{|I_{bat}(t_i+) - I_{bat}(t_i-)|} \quad (3)$$

The limitations of the method can be extracted directly from (3): once the batteries are equalized, there is no voltage difference among them, nor equalization current, meaning that R_i cannot be estimated this way. The SCE used in this paper (Fig. 1) equalizes based on voltage differences among cells, however, $LiFePO_4$ cells can have a rather flat OCV-SOC curve [12], so it may not achieve a perfect balance in terms of SOC. This is a limitation of the SCE employed in this paper. Nevertheless, this SCE can be used with any LIB technology with less flatness OCV-SOC [12]. Besides, and as stated in the introduction, this method can be combined with signal-injection based battery resistance estimation methods to estimate temperature. This would increase the reliability of the estimation, allowing to estimate the desired parameters even when the method proposed in this paper cannot be employed.

A. *Effect of inductive parasitic components*

As will be seen in section V, the circuitry has some unavoidable parasitic inductances due to e.g. cabling that affect the waveforms shown in Fig. 8b. This effect can be simulated by adding a small inductor (an inductor of 0.1nH has been used to emulate this effect) in series with C_{EQ} in Fig. 8a. The resulting waveforms are shown in Fig. 9. The orange waveform represents the response of the battery's voltage and current when the inductor is added to the circuit, in comparison with the blue waveforms that show the ideal case.

Since V_{bat} is measured at the battery terminals, the existence of this parasitic inductor does not affect the estimation of the IR. Any combination of voltage and current from the graph would result in the IR estimation. However, peak values are preferred since they provide a high signal-to-noise ratio. Equation (3) can be rewritten as (4), where $V_{batpeak}$ and $I_{batpeak}$ correspond to the peak values for current and voltage, respectively, right after t_i.

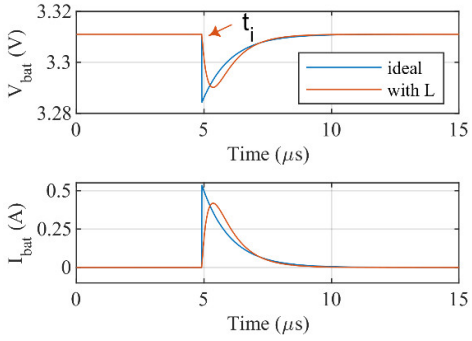

Fig. 9.- Resulting waveform from the simplified circuit in Fig. 8a comparing the ideal case (blue waveforms) with the case with a series inductor (orange waveforms).

$V_{batpeak}$ and $I_{batpeak}$ can be obtained from the derivatives of V_{bat} and I_{bat} respectively, which can be approximated by (5) using the Euler approximation, where X_{bat} represents either the current or the voltage, X'_{bat} represents either the discrete-time derivative of the current or the voltage, k represents the current time instant and T_s is the sampling time. $V_{batpeak}$ and $I_{batpeak}$ are theoretically acquired when X'_{bat} is zero; in practice when there is a change in the sign of X'_{bat}.

$$R_i = \frac{|V_{bat}(t_i-) - V_{batpeak}|}{|I_{batpeak} - I_{bat}(t_i-)|} \quad (4)$$

$$X'_{bat} = \frac{X_{bat}(k) - X_{bat}(k-1)}{T_s} \quad (5)$$

B. *Battery Temperature Estimation*

It is generally expected [13], [20], [23] that the battery resistance decreases as temperature increases at low frequencies. In this region, the electrolyte and SEI dominate the behavior of the battery and follows the Arrhenius law [20]. However, it must be noted that the proposed method estimates the IR, R_i in Fig. 8, which is dominated by the metal collectors and leads [30], which resistances increase as temperature does [13], [23]. Hence, IR can be modeled as a linear function of the battery temperature (6), provided that the metallic part of the battery dominates the response. R_{bat0} is the battery resistance (R_i) at the room temperature (T_o), T_{bat} is the battery temperature and α_{bat} is the temperature coefficient; R_{batn0} and α_{bat} can be measured during a commissioning process. The battery temperature is finally estimated from (7).

It is finally noted that although the method proposed in this paper is evaluated for the classical topology, see Fig. 1a, it can be extended to any other switched-capacitor topology, see section II-A.

$$R_{bat} = R_{bat0}(1 + \alpha_{bat}(T_{bat} - T_0)) \quad (6)$$

$$T_{bat} = \frac{R_{bat} - R_{bat0}}{R_{bat0}\alpha_{bat}} + T_0 \quad (7)$$

V. Simulations

An SCE with two cells was implemented in Matlab/Simulink, see Fig. 10.

The equalizer main parameters are shown in Table III. Cells are implemented using the battery model from Simscape Electrical toolbox, with $LiFePO_4$ battery equivalent parameters. A 30% difference in SOC between cells is set as

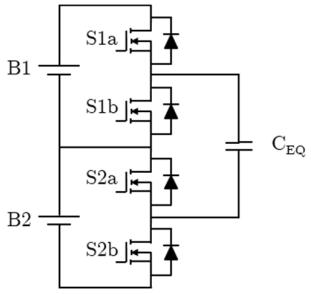

Fig. 10.- SCE with two batteries and one capacitor.

TABLE III. EQUALIZER AND BATTERY CHARACTERISTIC PARAMETERS.

Parameter	Value
Nominal battery voltage	3.2 V
Nominal current	3.2 A
Maximum charge current	1C
Maximum discharge current	3C
Battery capacity	3200 mAh
Equalizer capacitor	22 µF
IR (*Ri*)	50 mΩ

the initial condition: the most charged battery has an OCV of 3.312 V and the less charged one has an OCV of 3.284 V.

Fig. 11a shows the voltage and current of the most charged cell (B1 in Fig. 10) when it is connected in parallel to the balancing capacitor at t=5 µs. Voltage and current waveforms are seen to be in good agreement with the ones obtained with the Thèvenin model, see Fig. 8b. The estimated IR (2) is ≈50 mΩ, which matches R_i defined in Table III and included in the cell model for the simulation. The same results are obtained if the parasitic inductor is added in series with C_{eq} (Fig. 11b), as it was explained in section IV.A.

Simulation results with more than two cells have also been carried out. A simulation scenario with three cells (ideal case), see Fig. 1a, has been used, voltage and current are measured for B2, since this cell will share energy with both the upper (B1) and lower (B3) cells. SOCs of B1, B2 and B3 are 80%, 50% and 20% respectively. The resulting waveforms for a switching cycle (voltage ad current) can be seen in Fig. 12.

As expected, in the first half of the switching cycle B2 charges the bottom capacitor (C_{23}) since its voltage is higher than the one from B3. In the second half of the switching cycle, B2 receives energy from the upper capacitor (C_{12}),

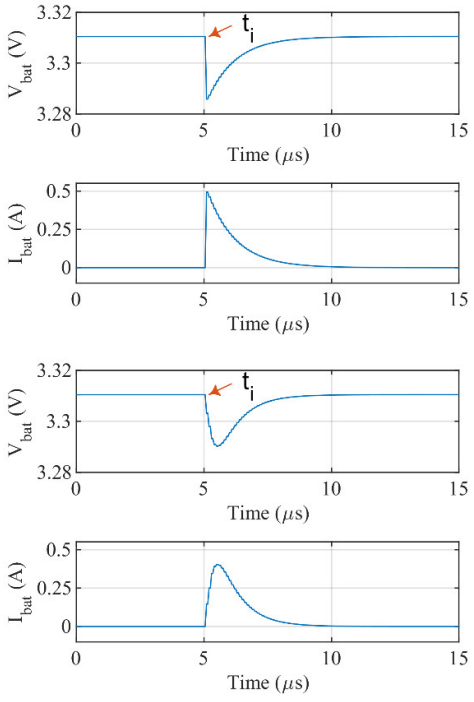

Fig. 11.- Resulting waveform from the equalizer, a) Simulink, ideal case, b) Simulink, case with the parasitic inductor (fs = 20kHz, SOC differences = 30%).

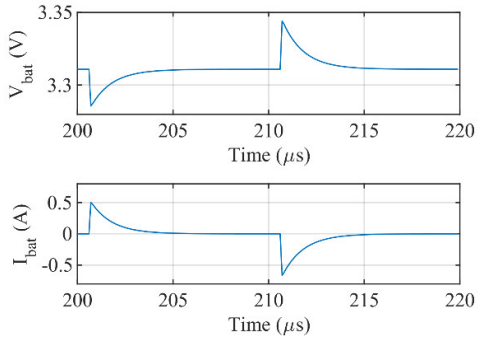

Fig. 12.- Voltage and current in one cycle for B2 cell in an SCE with 3 series-connected cells (see Fig. 1a).

since B1 has a higher voltage than B2. The cell IR can be calculated from any of these two transient responses with identical results. Different SOCs and arrangement of the cells would not interfere with the method either.

VI. Experimental Results

The SCE shown in Fig. 1c was used to carry out the experimental results. A two-cell arrangement has been used to be consistent with the simulation results shown in Section V. Current and voltage waveforms were measured with a Yokogawa 701932 current probe and with a Yokogawa 701938 voltage probe, respectively. Signals were captured with a Yokogawa 720250 12-bit 2-channel module plugged into a Yokogawa DL850 ScopeCoder. Parameters of the cell and SCE are shown in Table II.

In addition to the parameters shown in Table III, the Equivalent Series Resistance (ESR) of the equalization capacitor is 0.7 Ω [31]. This resistance will affect several aspects of the system: (i) it affects the equalization time and the efficiency of the equalization [11]; (ii) it will affect the sensitivity of the method, i.e. the bigger this resistance, the smaller will be the current peak and the highest the accuracy needed in the measurement system. It is also noted that the ON resistance of the MOSFETs will affect in a similar way; the ON resistance of the selected MOSFET is 2.4 mΩ [32]. In general, when designing an SCE, and since they are intended for low-cost applications, a good compromise among parasitic resistances, the overall performance of the components and cost must be achieved.

The $LiFePO_4$ cell used in this work is shown in Fig. 13a. Voltage measurement is performed at cell terminals. Cell voltage and current in one switching cycle are shown in Fig. 14. It can be seen that the current has a smoother response than in the ideal simulation (Fig. 11a), and similar to Fig. 11b, due to inductive parasitic components present in the actual system, as it was previously explained in section IV-A, hence (4) is used to estimate the IR.

The OCV-SOC curve of $LiFePO_4$ batteries is rather flat (see Fig. 13b) [12], meaning that the accuracy of the measurement system should be carefully analyzed. As stated in [12], a good target for SOC and IR estimation in these batteries would be in the range of 1-2 mV. The Least Significant Bit (LSB) indicates the resolution of an acquisition system and is the result of dividing the full-scale range (FSR) of the acquisition system by the number of discrete values obtained with n bits (8) [33]. With a 12 bits

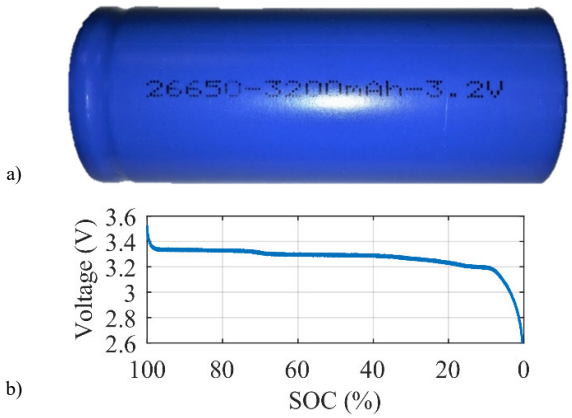

Fig. 13.- a) $LiFePO_4$ cell and b) OCV-SOC curve of the cell.

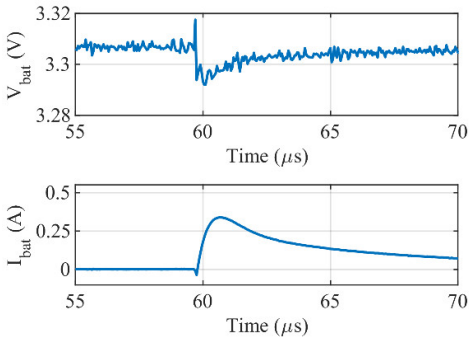

Fig. 14.- Experimental results (fs = 20kHz, T=20ºC, SOC differences = 30%).

resolution acquisition system, which is a common resolution in digital processors nowadays (e.g. DSPs), the LSB would be < 1 mV, which is in the recommended range in [12].

$$LSB = \frac{FSR}{2^n} \tag{8}$$

Besides, the method does not work when the cells are equalized within the LSB limit, see section IV. The LSB would be, then, the minimum threshold below where the proposed method would not work. In practice, this value will increases due to unavoidable noise in the real signals, as can be appreciated in Fig. 14. This methodology could be used with any LIB chemistries (not only in $LiFePO_4$ batteries which have the flattest profile among LIBs) [14]. It is finally noted that the voltage variation is expected to be always smaller than the current variation, so the current variation will not be a problem before the voltage variation is.

A. Resistance Variation With Switching Frequency

Switching frequency in an SCE can be optimized for a given capacity of the equalizing capacitors [34], in such a way that the capacitor can be fully charged/discharged during its switching cycle without staying charged/discharged for long before the next commutation. The maximum equalization frequency is related to the driver (driving the MOSFETs). In addition, increasing the switching frequency allows for a capacitor size reduction, but it also increases the switching losses in the MOSFETs, thus reducing the efficiency. In the case of the setup used in this paper (see Fig. 1d) the maximum switching frequency is ≈ 50 kHz.

Fig. 15 shows the estimated cell resistance for a set of experimental data captured with the SCE working at 10 kHz,

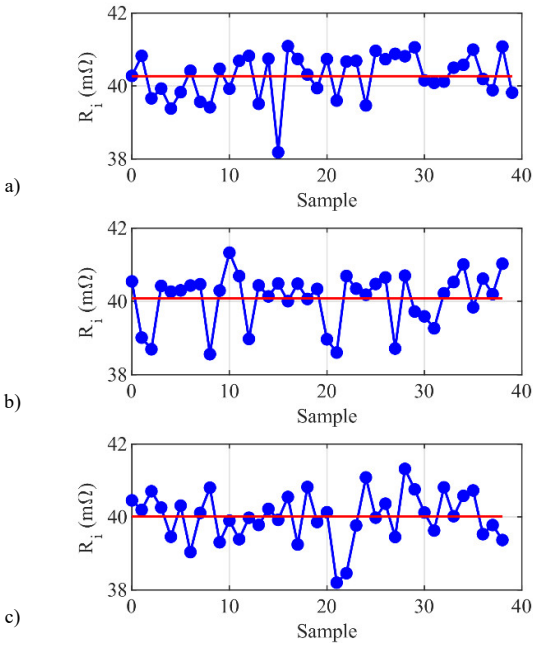

Fig. 15.- Cell 1 IR estimation using the experimental data collected from the equalizer (blue) and mean value of the estimated resistance (red): a) 10 kHz, b) 20 kHz, and c) 30 kHz.

20 kHz and 30 kHz; the mean value of the estimated cell resistance is shown in red.

The mean value at all the frequencies of the estimated resistances shown in Fig. 15 is similar at all the frequencies since the resistance being estimated is R_i, which depends on the voltage/current at the switching instant, which is independent of the SCE switching frequency. It is also noted that SOC, SOH or temperature time constants are significantly larger than battery resistance estimation time [35], meaning that averaging the measurements for a certain period could be an acceptable and easy solution to reject

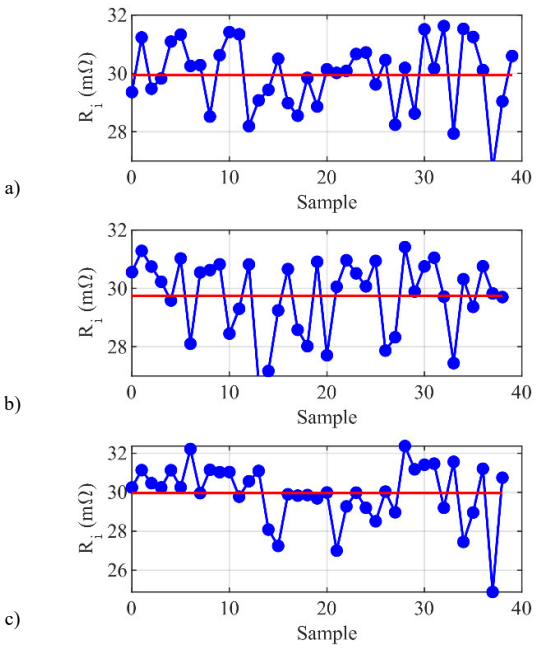

Fig. 16.- Cell 2 IR estimation using the experimental data collected from the equalizer (blue) and mean value of the estimated resistance (red), a) 10kHz, b) 20kHz, c) 30kHz.

measurement noise. Experimental results are repeated with another cell (see Fig. 16) with the same characteristics, to show the replicability of the methodology. It is shown that the R_i mean value is independent of the switching frequency. However, the absolute value of R_i is different: for the first cell the mean value of R_i is ≈ 40 mΩ, while for the second one is ≈ 30 mΩ. This was expected due to differences among cells existing in practice [7], [8].

B. Resistance Variation With Temperature

Fig. 17 shows the estimated IR for three different cells as the temperature increases. The cells are slowly heated (for around 45 minutes, see Fig. 18) up to 65ºC while capturing current, voltage and temperature. The temperature of the cells is monitored using LM35 temperature sensors [36], placed on the surface of the cell. It can be observed from Fig. 17 how the cell resistance increases almost linearly with temperature for all tested cells.

It can be observed from Fig. 17 that, although there is an offset among IRs, the rate of variation of IR with temperature is similar for all cells under test. Offsets present among cells will not affect the accuracy of the proposed method because the cell temperature will be estimated from variations of the resistance with temperature respect to the room temperature resistance (R_{bat0}) as seen in (7).

Fig. 19 shows the measured and estimated temperature using (7). First, the slope that best fits the temperature variation for each of the three cells was obtained (see table IV), then, the average value of this slope (α_{bat} = 16.72 1/ºC) is used to estimate the temperature for all cells under test. The temperature estimation error for the three cells analyzed is shown in Fig. 20; the temperature estimation error is seen to be less than ≈ 12º C for any point, with a mean value of 4ºC and a standard deviation of 4.11ºC. Due to this difference, it is important to analyze more than one point every time, as seen in Fig. 15 and Fig. 16, so the conclusions in terms of temperature are valid.

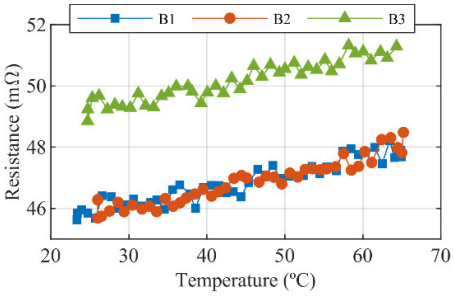

Fig. 17.- Cell resistance vs. cell temperature for different cells.

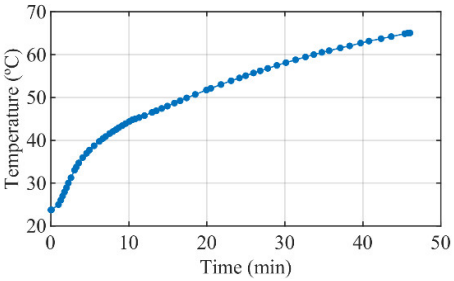

Fig. 18.- Temperature evolution of the cell with time.

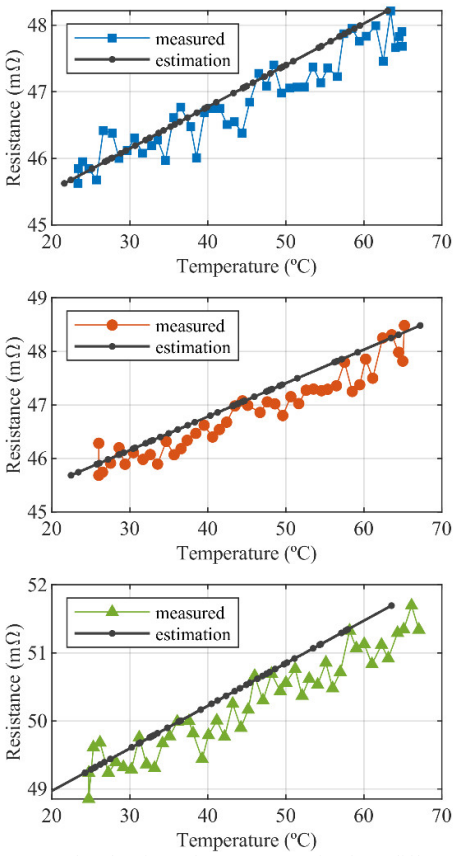

Fig. 19.- Measured and estimated temperatures for three different cells, a)-c) B1-B3.

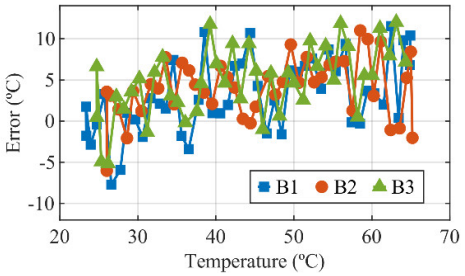

Fig. 20.- Error between measured and estimated temperature.

TABLE IV: THERMAL COEFFICIENTS FOR THE DIFFERENT CELLS EVALUATED

Cell	Thermal coefficient α_{bat} (1/ºC)
1 (blue in Fig. 19)	0.057
2 (orange in Fig. 19)	0.0626
3 (green in Fig. 19)	0.0601
Average	0.0598

VII. CONCLUSIONS

This paper proposes the use of signals naturally produced by SCEs to estimate the battery IR. The method operates without interfering with the regular operation of both the equalizer and battery and is valid for a wide range of switching frequencies. The IR estimate can be used to obtain the battery's temperature. However, its main limitation is that once the cells are equalized the IR cannot be estimated. Experimental results have been provided to demonstrate the viability of the proposed method.

VIII. Acknowledgment

The authors wish to acknowledge the support and motivation provided by the University of Oviedo, Spain, and Electrotécnica Industrial y Naval, S.L. (ELINSA), Spain.

References

[1] C. G. Moral, D. F. Laborda, L. S. Alonso, J. M. Guerrero, D. Fernández, C. Rivas and D. Reigosa, "Battery internal resistance estimation using a battery balancing system based on switched capacitors," IEEE Energy Conversion Congress and Exposition (ECCE), Baltimore, MD, USA, pp. 2516-2522, Sept. 2019.

[2] D. Anseán, M. González, V. M. García, J. C. Viera, J. C. Antón and C. Blanco, "Evaluation of $LiFePO_4$ batteries for electric vehicle applications," IEEE Transaction on Industrial Application, vol. 51, no. 2, pp. 1855-1863, March-April 2015.

[3] Z. Miao, L. Xu, V. R. Disfani and L. Fan, "An SOC-based battery management system for microgrids," IEEE Transactions on Smart Grid, vol. 5, no. 2, pp. 966-973, March 2014.

[4] J.P. Fellner, G.J. Loeber, S.P. Vukson, C.A. Riepenhoff, "Lithium-ion testing for spacecraft applications," Journal of Power Sources, vol. 119–121, pp. 911-913, June 2003.

[5] G. Pistoia, "In battery operated devices and systems," Elsevier, Amsterdam, 2009.

[6] E. Chemali, M. Preindl, P. Malysz and A. Emadi, "Electrochemical and Electrostatic Energy Storage and Management Systems for Electric Drive Vehicles: State-of-the-Art Review and Future Trends," in IEEE Journal of Emerging and Selected Topics in Power Electronics, vol. 4, no. 3, pp. 1117-1134, Sept. 2016.

[7] J. Cao, N. Schofield and A. Emadi, "Battery balancing methods: A comprehensive review," IEEE Vehicle Power and Propulsion Conference, Harbin, pp. 1-6, Sept. 2008.

[8] W. F. Bentley, "Cell balancing considerations for lithium-ion battery systems," The Twelfth Annual Battery Conference on Applications and Advances, Long Beach, CA, USA, 1997, pp. 223-226.

[9] Z. Yang, D. Patil and B. Fahimi, "Electrothermal Modeling of Lithium-Ion Batteries for Electric Vehicles," in IEEE Transactions on Vehicular Technology, vol. 68, no. 1, pp. 170-179, Jan. 2019.

[10] S. W. Moore and P. J. Schneider, "A review of cell equalization methods for lithium ion and lithium polymer battery systems," SAE Technical Paper, March 2001.

[11] M. Kim, C. Kim, J. Kim and G. Moon, "A Chain structure of switched capacitor for improved cell balancing speed of Lithium-Ion batteries," IEEE Transactions on Industrial Electronics, vol. 61, no. 8, pp. 3989-3999, Aug. 2014.

[12] H. Rahimi-Eichi, U. Ojha, F. Baronti and M. Chow, "Battery management system: An overview of its application in t he smart grid and electric vehicles," IEEE Industrial Electronics Magazine, vol. 7, no. 2, pp. 4-16, June 2013.

[13] A. E. Mejdoubi, H. Gualous, H. Chaoui and G. Alcicek, "Experimental investigation of calendar aging of lithium-ion batteries for vehicular applications," EMC Conference, Turkiye, Ankara, pp. 1-5, Sept. 2017.

[14] C. Pascual and P. T. Krein, "Switched capacitor system for automatic series battery equalization," Proc. IEEE 1997 Applied Power Electronics Conference, pp. 848-854, Feb. 1997.

[15] Y. Ye, K. W. E. Cheng, Y. C. Fong, X. Xue and J. Lin, "Topology, modeling, and design of switched-capacitor-based cell balancing systems and their balancing exploration," IEEE Transactions on Power Electronics, vol. 32, no. 6, pp. 4444-4454, June 2017.

[16] A. C. Baughman and M. Ferdowsi, "Double-tiered switched-capacitor battery charge equalization technique," IEEE Transactions on Industrial Electronics, vol. 55, no. 6, pp. 2277-2285, June 2008.

[17] Y. Shang, N. Cui, B. Duan and C. Zhang, "Analysis and optimization of star-structured switched-capacitor equalizers for series-connected battery strings," IEEE Transactions on Power Electronics, vol. 33, no. 11, pp. 9631-9646, Nov. 2018.

[18] Y. Shang, C. Zhang, N. Cui and C. C. Mi, "A delta-structured switched-capacitor equalizer for series-connected battery strings," IEEE Transactions on Power Electronics, vol. 34, no. 1, pp. 452-461, Jan. 2019.

[19] R. R. Richardson, P. T. Ireland, D. A. Howey, "Battery internal temperature estimation by combined impedance and surface temperature measurement," Journal of Power Sources, vol. 265, pp. 254-261, Nov. 2014.

[20] N. S. Spinner, C. T. Love, S. L. Rose-Pehrsson, S. G. Tuttle, "Expanding the Operational Limits of the Single-Point Impedance Diagnostic for Internal Temperature Monitoring of Lithium-ion Batteries," Electrochimica Acta, vol. 174, pp. 488-493, August 2015.

[21] C. Gonzalez Moral, D. Fernandez, J. M. Guerrero, D. Reigosa, C. Rivas and F. Briz, "Thermal monitoring of $LiFePO_4$ batteries using switching harmonics," in IEEE Transactions on Industry Applications, doi: 10.1109/TIA.2020.2988425.

[22] J. G. Zhu, Z. C. Sun, X. Z. Wei, and H. F. Dai, "A new lithium-ion battery internal temperature on-line estimate method based on electrochemical impedance spectroscopy measurement," Journal of Power Sources, vol. 274, pp. 990-1004, Jan. 2015.

[23] J. P. Schmidt, S. Arnold, A. Loges, D. Werner, T. Wetzel, E. Ivers-Tiffée, "Measurement of the internal cell temperature via impedance: Evaluation and application of a new method," Journal of Power Sources, vol. 243, pp. 110-117, Dec. 2013.

[24] D. Ansean, M. Gonzalez, J. C. Viera, V. M. Garcia, J. C. Alvarez and C. Blanco, "Electric vehicle Li-Ion battery evaluation based on internal resistance analysis," IEEE Vehicle Power and Propulsion Conference (VPPC), Coimbra, pp. 1-6, Oct. 2014.

[25] Y. Yuanmao, K. W. E. Cheng and Y. P. B. Yeung, "Zero-current switching switched-capacitor zero-voltage-gap automatic equalization system for series battery string," IEEE Transactions on Power Electronics, vsol. 27, no. 7, pp. 3234-3242, July 2012.

[26] Min Chen and G. A. Rincon-Mora, "An accurate electrical battery model capable of predicting runtime and I-V performance," IEEE Transactions on Energy Conversion, vol. 21, no. 2, pp. 504-511, June 2006.

[27] B. Pattipati, C. Sankavaram and K. Pattipati, "System Identification and Estimation Framework for Pivotal Automotive Battery Management System Characteristics," IEEE Transactions on Systems, Man, and Cybernetics, Part C (Applications and Reviews), vol. 41, no. 6, pp. 869-884, Nov. 2011.

[28] S. Buller, M. Thele, E. Karden, R. W. D. Doncker, "Impedance-based non-linear dynamic battery modeling for automotive applications," Journal of Power Sources, vol. 113, no. 2, pp. 422-430, Jan. 2003.

[29] B. Schweighofer, K. M. Raab and G. Brasseur, "Modeling of high power automotive batteries by the use of an automated test system," IEEE Transactions on Instrumentation and Measurement, vol. 52, no. 4, pp. 1087-1091, Aug. 2003.

[30] M. A. Roscher, D. U. Sauer, "Dynamic electric behavior and open-circuit-voltage modeling of $LiFePO_4$-based lithium ion secondary batteries," Journal of Power Sources, vol. 196, pp. 331-336, Jan. 2011.

[31] KEMET, "Tantalum Surface Mount Capacitors – Standard Tantalum: T491 Industrial Grade MnO2," Feb. 2020. Available: https://content.kemet.com/datasheets/KEM_T2005_T491.pdf, accessed 04-April-2020.

[32] INFINEON, "IRLB8314PbF datasheet," Aug. 2018. Available: https://www.infineon.com/dgdl/irlb8314pbf.pdf?fileId=5546d462533600a4015356604d6f258f, accessed 04-April-2020.

[33] B. Widrow, I. Kollar and M. C. Liu, "Statistical theory of quantization," in IEEE Transactions on Instrumentation and Measurement, vol. 45, no. 2, pp. 353-361, Apr. 1996.

[34] Y. Ye and K. W. E. Cheng, "Modeling and Analysis of Series–Parallel Switched-Capacitor Voltage Equalizer for Battery/Supercapacitor Strings," in IEEE Journal of Emerging and Selected Topics in Power Electronics, vol. 3, no. 4, pp. 977-983, Dec. 2015.

[35] Y. Zou, X. Hu, H. Ma and S. E. Li, "Combined State of Charge and State of Health estimation over lithium-ion battery cell cycle lifespan for electric vehicles," Journal of Power Sources, Volume 273, pp. 793-803, Jan. 2015.

[36] Texas Instruments, LM35 Precision Centigrade Temperature Sensors datasheet, August, 1999. Revised Dec, 2017.